Random pinning in glassy spin models with plaquette interactions

Robert L. Jack, Ludovic Berthier

PHYSICAL REVIEW E **85**, 021120 (2012)

Random pinning in glassy spin models with plaquette interactions

Robert L. Jack[1] and Ludovic Berthier[2]
[1]*Department of Physics, University of Bath, Bath, BA2 7AY, United Kingdom*
[2]*Laboratoire Charles Coulomb, UMR 5221, CNRS and Université Montpellier 2, F-34095 Montpellier, France*
(Received 10 December 2011; published 15 February 2012)

We use a random pinning procedure to study amorphous order in two glassy spin models. On increasing the concentration of pinned spins at constant temperature, we find a sharp crossover (but no thermodynamic phase transition) from bulk relaxation to localization in a single state. At low temperatures, both models exhibit scaling behavior. We discuss the growing length and time scales associated with amorphous order, and the fraction of pinned spins required to localize the system in a single state. These results, obtained for finite dimensional interacting models, provide a theoretical scenario for the effect of random pinning that differs qualitatively from previous approaches based either on mean-field, mode-coupling, or renormalization group treatments.

DOI: 10.1103/PhysRevE.85.021120 PACS number(s): 05.20.Jj, 05.10.Ln, 64.70.qd

I. INTRODUCTION

Supercooled liquids and glasses have very large relaxation times and complex relaxation mechanisms, but their structures appear disordered and unremarkable [1–3]. This combination is surprising and rather mysterious, especially because several recent studies [4–6] indicate that if a relaxation time increases sufficiently rapidly on cooling then this must be accompanied by the development of some kind of structural order. The idea of growing amorphous order is that the diversity of amorphous states, as quantified by the configurational part of the entropy, decreases at low temperatures. This leads to increasing static correlation length scales, which can be measured using point-to-set correlations [4–10]. If these length scales are large, the system may be localized into a single amorphous state by fixing the positions of a small fraction of the particles [11,12]. This localization occurs at temperatures above the glass transition temperature, so the pinning procedure bypasses the challenging task of thermalizing systems at very low temperatures.

Here, we investigate amorphous order in two finite dimensional interacting spin systems. These are the square plaquette model (SPM) [13] and the triangular plaquette model (TPM) [14]. They both have growing relaxation times at low temperatures, but two-point thermodynamic correlation functions do not indicate the presence of any growing length scale [15], and the models do not have phase transitions at any finite temperature. Additionally, structural relaxation at low temperatures exhibits strong dynamical heterogeneity and growing dynamic length scales [16,17]. These features mimic those of supercooled liquids, but the models are numerically and analytically more tractable than off-lattice particle systems. This makes them useful models for studying generic features of glassy systems [16–19].

Several methods have been proposed for characterizing amorphous order. A prominent recent example is to fix particles everywhere except within a small cavity, and then to study the motion of particles within this cavity [4,7,8,11,20]. Other possible measurements of amorphous order involve freezing spins in a different geometrical arrangement [9,11], or direct measurement of the diversity of amorphous packings [6,20–22]. Here we follow [11,12,23–25] and fix a fraction f of particles (or spins), distributed randomly through the system in the positions (or orientations) that are representative of thermal equilibrium. In supercooled liquids, a thermodynamic phase transition on varying f was recently predicted [12], based on an analysis within random first-order transition (RFOT) theory [26,27]. Another recent analysis based on mode-coupling theory predicts a dynamic singularity on varying f [28]. Numerical studies [11,23–25] have mainly addressed the behavior at low to moderate pinning fraction f, leaving open the question of the existence of phase transitions at larger f.

Here, we explore the effect of random pinning in the plaquette models, concentrating on the behavior at the relatively large pinning fractions where phase transitions are predicted to occur in supercooled liquids. We show that the plaquette models do not exhibit thermodynamic phase transitions on varying f at any finite temperature. However, we do find a well-defined crossover from "bulk" behavior (where the system explores a large number of configurations), to "frozen" behavior (where the system remains trapped in a region of configuration space) occurring at some finite fraction f^*. As the temperature is reduced, the crossover occurs at an increasingly small value of f^*, and becomes increasingly sharp.

From previous studies of point-to-set correlations in closed cavities for plaquette models [17], it is known that these models do have growing amorphous order at low temperatures, but their behavior is not consistent with RFOT. The results we present here therefore illustrate a theoretical scenario, alternative to mode-coupling and RFOT treatments, for understanding the behavior of model supercooled liquids with randomly pinned particles. Presumably a similar conclusion would hold in the context of models with avoided critical points where growing static length scales are predicted to exist without yielding ideal glass transitions [29,30].

After defining our models in Sec. II, we show numerical results for the bulk-to-localized crossover in Sec. III. In Sec. IV we investigate the length scales that characterize amorphous order in the system, including their scaling with temperature. In Sec. V we use analytic arguments in the SPM to study the small-f behavior, and the behavior near the crossover. Finally in Sec. VI we discuss the interpretation of our results, including their relation to previous theoretical analysis.

II. PLAQUETTE MODELS

A. Definitions

The plaquette models consist of Ising spins, $s_i = \pm 1$, on a lattice, interacting through either three- or four-body terms. They evolve dynamically through single spin flips with Metropolis rates, $w_i = \min(1, e^{-\beta \Delta E_i})$, where ΔE_i is the change in energy of the system on flipping spin i and $\beta \equiv 1/T$ is the inverse temperature.

The energy of the square plaquette model (SPM) is

$$E = -\frac{1}{2} \sum_{\square} s_1 s_2 s_3 s_4, \tag{1}$$

where the sum runs over plaquettes of the square lattice [13,15]. It is useful to define $c \equiv e^{-\beta}$, since length and time scales typically show power-law scaling with c in the low-temperature limit ($c \to 0$). The model has a dual representation in terms of "defect" variables, $n_p = (1 - s_1 s_2 s_3 s_4)/2$, which are associated with the plaquettes p of the square lattice. In terms of these defect variables, the thermodynamic properties of the system are those of a noninteracting lattice gas with $\langle n_p \rangle = (1 + e^{\beta})^{-1}$ approximately equal to c at low temperatures. We use square systems with periodic boundaries.

The energy of the triangular plaquette model (TPM) is

$$E = -\frac{1}{2} \sum_{\nabla} s_1 s_2 s_3, \tag{2}$$

where the sum runs over downward pointing plaquettes of the hexagonal lattice [14]. In this model, the defect variables are associated with these plaquettes, $n_p = (1 - s_1 s_2 s_3)/2$. We use rhombus-shaped systems with periodic boundaries. We always take the linear system size to be a power of 2, which minimizes finite-size effects.

In the defect representation, both the SPM and the TPM have strong similarities with kinetically constrained models [31]. In both systems, the thermodynamic free energy per spin (in the limit of large systems) is simply $-T \log[2 \cosh(1/2T)]$. This is a smooth and unremarkable function of temperature down to $T = 0$. However, the dynamical properties of the models, to be described shortly, are not trivial. This combination of simple thermodynamic properties and complex dynamics is consistent with the dynamic facilitation picture of the glass transition [32].

B. Square plaquette model at $f = 0$

Before considering the effect of pinning a fraction of spins, we first review some relevant results for the SPM with $f = 0$; see Refs. [15,16] for more details. Symmetry under global spin reversal implies that $\langle s_i \rangle = 0$, and all nontrivial two-point and three-point correlation functions also vanish. The simplest nontrivial correlation functions involve four spins. For spins a,b,c,d lying on the four vertices of an $x \times y$ rectangle then

$$g_{\rm s}(x,y) \equiv \langle s_a s_b s_c s_d \rangle_0 = \tanh(\beta/2)^{xy}. \tag{3}$$

All other nontrivial four-point correlations vanish.

The function $g_{\rm s}(x,y)$ has scaling behavior at low temperatures. Full details are given in Sec. IV B below, but the essential points are that correlations are anisotropic and the model supports two correlation lengths at low temperatures. The shorter length is $\xi_0 \sim c^{-1/2}$, and there is also a longer length $\xi \sim c^{-1}$ associated with the correlations along the lattice axis. We note that previous analysis of static correlations considered only the shorter of these two correlation lengths [16].

Point-to-set correlations were considered in Ref. [17], for the case of an isotropic (square) cavity of linear size r. For $r \lesssim \xi_0 \sim c^{-1/2}$, the configurational entropy of the cavity is close to zero. For $\xi_0 \lesssim r \lesssim \xi \sim c^{-1}$, the cavity has strong finite-size effects but its configurational entropy is nonzero and the spin-spin autocorrelation function decays to zero at the center of the cavity. This implies that these larger cavities are no longer frozen in a single amorphous state, so we identify ξ_0 as the point-to-set length [17].

Dynamical observables in the square plaquette model also show scaling behavior. The relaxation time for spins is $\tau \approx c^{-3} \sim e^{3/T}$, consistent with the behavior of "strong" glass formers [18]. Energy-energy correlations decay have relaxation times longer than τ at low temperatures, although they also have Arrhenius scaling. Four-point dynamic correlation functions, also discussed in more detail below, are anisotropic as well, with correlations being strongly localized along the axis of the square lattice, and having spatial on-axis extension of range $\xi \sim e^{\beta} = c^{-1}$ [16].

C. Triangular plaquette model at $f = 0$

Static correlations in the TPM were discussed in Ref. [14] where it was shown that $\langle s_i \rangle = 0$ and $\langle s_i s_j \rangle = \delta_{ij}$, as in the SPM. The relaxation time in the TPM has "fragile" superarrhenius scaling $\tau \sim e^{1/(T^2 \log 3)}$ [17], which arises from a hierarchy of mechanisms whose characteristic time scales increase as the logarithm of their associated length scales (see also [33–35]). Static correlation lengths, point-to-set correlations, and dynamical four-point correlations are considered in Ref. [17], where it was found that the scaling of these functions all depend on a unique correlation length scale, $\xi \sim c^{-1/d_{\rm f}}$, where $d_{\rm f} = \log 3/\log 2 \approx 1.585$ is the fractal dimension of the Sierpinski triangle. It was also found recently [36] that the TPM supports unusual phase transitions if it is constrained to have a fixed nonzero magnetization, but we do not discuss that case here.

III. EFFECT OF RANDOM PINNING

We now turn to our main results, which correspond to the following thought experiment [11,12,23,24,28,37]. We select a reference configuration from a thermally equilibrated system and we instantaneously "freeze" (or "pin") at time $t = 0$ the state of a finite set of spins. Each spin is frozen with probability f, independently of all other spins. The spins that are not frozen evolve with Monte Carlo (MC) dynamics for some time t, after which various measurements are performed.

A. Correlation functions and susceptibilities

To describe these measurements, we first establish our notations and define the correlation functions and susceptibilities that we will consider. The system consists of V spins $s_i = \pm 1$, with $i = 1, \ldots, V$. To describe whether a spin is frozen, we introduce the binary variables f_i, with $f_i = 1$ if spin i is

frozen, zero otherwise. We use angle brackets $\langle\cdots\rangle$ to denote averages which run over the reference configuration, the choice of frozen spins, and the MC dynamics. We also use $\langle\cdots\rangle_0$ to denote a "bulk" thermal average, that is, in the absence of any pinned particles ($f = 0$).

It is convenient to define the autocorrelation of the mobile spins. For spin i, this is defined as $a_i(t) = (1 - f_i)s_i(t)s_i(0)$, and it takes values $0, \pm 1$. The number of mobile (unfrozen) spins is $\hat{N}_{\rm m} = \sum_i (1 - f_i)$, which is a fluctuating quantity within our analysis. We also define the (extensive) overlap $\hat{Q}(t) = \sum_i a_i(t)$ and the (intensive) autocorrelation function,

$$C(t) = \frac{\langle \hat{Q}(t)\rangle}{\langle \hat{N}_{\rm m}\rangle} = \frac{\langle a_i(t)\rangle}{1 - f}. \tag{4}$$

The four-point susceptibility quantifies the strength of spontaneous fluctuations of the overlap,

$$\chi_4(t) = \frac{\langle \delta\hat{Q}(t)^2\rangle}{\langle \hat{N}_{\rm m}\rangle} = \frac{\sum_j g_{4,ij}(t)}{1 - f}, \tag{5}$$

and it is related to the volume integral of the four-point correlation function defined as

$$g_{4,ij}(t) = \langle \delta a_i(t)\delta a_j(t)\rangle. \tag{6}$$

We use the notation $\delta O = O - \langle O\rangle$ for thermal fluctuations throughout this article.

In addition to the usual four-point correlations, we introduce three-point correlations and susceptibilities. We measure how the positions of the pinned spins are correlated with the states of mobile spins through the correlation,

$$X_{ij}(t) = \langle \delta a_i(t)\delta f_j\rangle. \tag{7}$$

The ratio (X_{ij}/f) measures the change in the average of a_i if spin j is assumed to be frozen. Hence,

$$\frac{\partial C(t)}{\partial f} = \frac{1}{f(1 - f)^2}\sum_{j\neq i} X_{ij}. \tag{8}$$

To prove this relation, one writes $f = (1 + e^{\mu})^{-1}$, so that $\langle a_i(t)\sum_j \delta f_j\rangle = -\frac{\partial}{\partial\mu}\langle a_i(t)\rangle$, and Eq. (8) follows.

It is interesting to note that $X_{ij}(t)$ is an example of a three-point correlation function, and that $\frac{\partial C(t)}{\partial f}$ is therefore a three-point susceptibility, in the spirit of the dynamic functions introduced in Refs. [38,39]. Following Refs. [38–40] we can obtain a lower bound $\Delta\chi_4$ on the four-point susceptibility, $\chi_4(t) \geqslant \Delta\chi_4(t)$, which involves the three-point susceptibility defined above as

$$\Delta\chi_4(t) = f\left[(1 - f)\frac{\partial C(t)}{\partial f} - C(t)\right]^2. \tag{9}$$

This relation is proved in the Appendix where we also show that a sufficient condition for saturation of the bound [i.e., $\chi_4(t) = \Delta\chi_4(t)$] is that for a given choice of frozen spins, the autocorrelations of the mobile spins are independent of each other and depend separately on the individual f_j. When this condition is obeyed, then the four-point correlation function may be expressed as a convolution of X_{ij} with itself:

$$g_{4,ij}(t) \approx \frac{1}{f(1 - f)}\sum_k X_{ik}(t)X_{jk}(t). \tag{10}$$

We refer to the Appendix for more details on this particular point.

Of particular interest is the limit of large time, $t \to \infty$, in which correlation functions become independent of the dynamical evolution of the system and may be calculated by equilibrium statistical mechanics. In this limit, we drop the time argument on our correlation functions, writing, as $t \to \infty$: $C(t) \to q$, $g_{4,ij}(t) \to g_{4,ij}$, $X_{ij}(t) \to X_{ij}$, and $\chi_4(t) \to \chi_4$. These limiting quantities are given by "static" correlation functions. A general recipe for calculating them is given in the Appendix, which follows a similar analysis for off-lattice particle systems [41]. For small f, in particular, they may be calculated in a series expansion; see also Sec. V.

B. Numerical results

An overview of the influence of pinned spins on the SPM is shown in Fig. 1. In Fig. 1(a) we show that as f is increased from zero, the long-time limit of $C(t)$ increases monotonically, since the frozen spins tend to maintain the system close to its initial state, preventing full relaxation of the autocorrelation function of the mobile spins. Thus, we confirm that by randomly freezing spins, the system crosses over from "bulk" ergodic relaxation for $f = 0$ to a nearly "frozen" state at large f. Our goal is now to characterize this crossover further.

In Fig. 1(b), we show the evolution of $q = q(f,T)$ with the fraction of pinned spins and temperature. As expected from Fig. 1(a), the static value of the overlap increases monotonically with f at any given temperature. More interesting is the temperature dependence of the $q(f,T)$ curves. We find that q increases rapidly with decreasing temperature at constant f. This implies that for lower temperatures, a smaller amount of random pinning is required to localize the system in a single state. The interpretation is that the system has a greater degree of amorphous order at low temperatures.

Looking more closely at the f dependence of q, the data in Fig. 1(b) indicate that $q(f,T)$ has an inflexion point at a characteristic value of the pinning fraction, $f = f^*$, so that the susceptibility $(\partial q/\partial f)$ is small both for small f and for large f, with a well-defined maximum at $f^*(T)$. Thus we find that the bulk-to-localized crossover obtained with random pinning can be located by measuring the derivative of the static overlap. However, anticipating the discussion in Sec. VI, we note that $q(f,T)$ is a smooth function of f with no sign of the sharp discontinuity that would be observed at a first-order phase transition [12].

We next turn to fluctuations of the overlap, which we quantify via the four-point susceptibility $\chi_4(t)$. In Fig. 1(c), we show the time evolution of $\chi_4(t)$ for different values of f, at constant temperature. For $f = 0$, the susceptibility $\chi_4(t)$ has a peak for $t \approx \tau$, as usual in glassy systems [10]. However, two features emerge when f is increased. First, the time dependence changes dramatically: The maximum in $\chi_4(t)$ shifts to longer times until, for large f, the susceptibility $\chi_4(t)$ is monotonically increasing and saturates to a plateau at long times. This long time limit corresponds to the static susceptibility $\chi_4 = \chi_4(f,T)$, proportional to the variance in the overlap $q(f,T)$. This increasing static susceptibility indicates that deviations between the final configuration and the initial (reference) configuration appear by cooperative

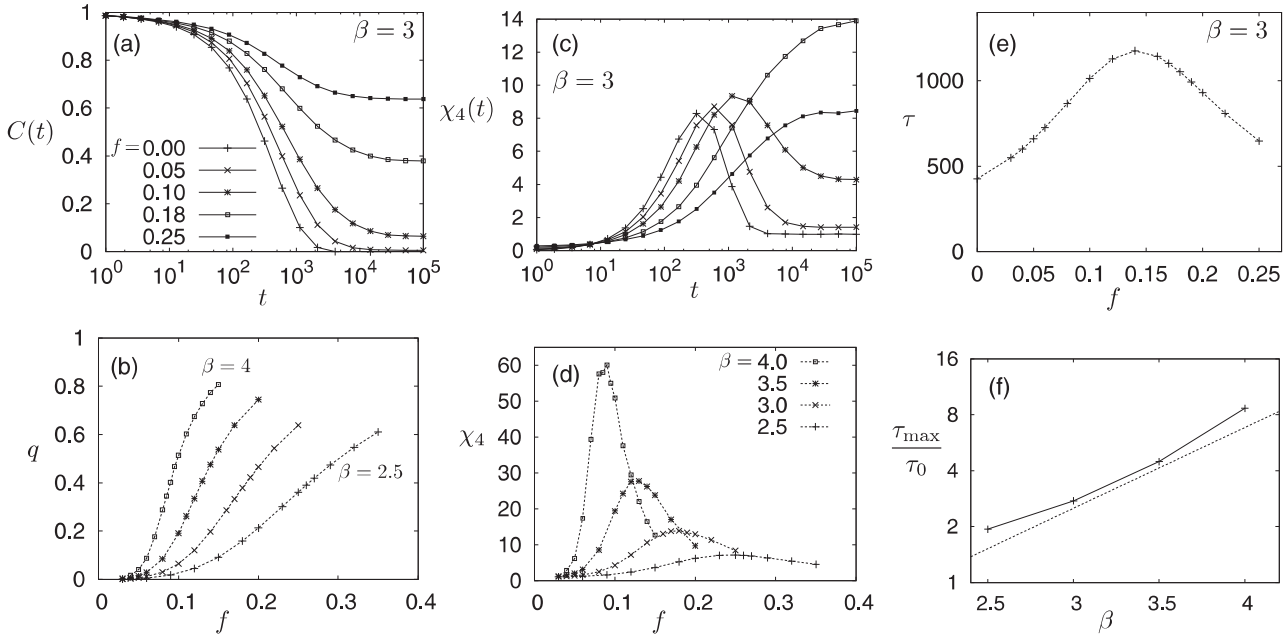

FIG. 1. Overview of behavior of the SPM with pinned spins. (a) Time-dependent correlation function $C(t)$ at inverse temperature $\beta = 3$. (b) The long-time overlap $q = \lim_{t\to\infty} C(t)$ as a function of pinning fraction f for four temperatures [the symbols are the same as those in panel (d)]. (c) Time-dependent four-point susceptibility $\chi_4(t)$ at $\beta = 3$. (d) Long-time limit of χ_4, for various temperatures. (e) Behavior of the relaxation time on varying f at $\beta = 3$. (f) Behavior of the maximal relaxation time $\tau_{\max} = \max_f \tau(f)$, normalized by the bulk relaxation time $\tau_0 = \tau(f = 0)$, as a function of inverse temperature. In practice $\tau_{\max} \approx \tau(f^*)$. The straight line is $\tau_{\max}/\tau_0 \propto e^{\beta}$ which would imply $\tau_{\max} \propto e^{4\beta}$. It is clear from the upward curvature of the numerical data that $\tau_{\max}$ has a super-Arrhenius temperature dependence.

processes involving many spins. Just like $(\partial q/\partial f)$, the static susceptibility χ_4 goes through a maximum at the characteristic pinning fraction f^*.

Physically, the interpretation of the behavior of $\chi_4(t)$ is as follows. When $f \ll f^*$, the system is in the bulk regime and easily escapes from the reference state through a process that is not very different from bulk relaxation. In this case, $\chi_4(t)$ is large near $t \approx \tau$, but it is small at long times since initial and final states are very different. When $f \gg f^*$, by contrast, there are so many frozen spins that the system is very constrained and few spins can relax. While the overlap is large, its fluctuations are necessarily quite small. For $f \approx f^*$, the number of frozen spins is just large enough to maintain the system near its initial state, and the overlap exhibits stronger fluctuations because the system "hesitates" between both possibilities ("*should I stay or should I go*"). We discuss the spatial structure of these correlations in Sec. IV below.

We show in Fig. 1(d) the evolution of the static susceptibility χ_4 with f for different temperatures. As anticipated, the susceptibility goes through a maximum whose location and amplitude are strong functions of the temperature. On going to lower temperature, the peak of χ_4 remains located near $f = f^*$ so it shifts toward smaller values of f; the amplitude of the peak increases rapidly, and its width decreases. Thus, the crossover between bulk and localized behaviors becomes sharper and more pronounced at low temperatures. A relevant conclusion for supercooled liquids is that the data in Fig. 1(d) show an increasing static susceptibility that measures the growth of amorphous order, but these data are obtained without any *a priori* knowledge of the many-body correlations that are responsible for this order. Thus, the random pinning procedure is a generic way to measure a growing static susceptibility in liquids approaching the glass transition, and offers a thermodynamic alternative to the measurement of relevant length scales via dynamic heterogeneity.

Turning to the dynamic behavior in the presence of random pinning, we define a relaxation time $\tau = \tau(f,T)$ from the time decay of $C(t)$, via $\frac{C(\tau)-q}{1-q} = 1/e$. We compute τ using the data shown in Fig. 1(a) and show the results in Fig. 1(e). We also find that τ has a nonmonotonic behavior, the relaxation being slowest near f^*. While the maximum is not very pronounced in Fig. 1(e), we show in Fig. 1(f) that the ratio $\tau(f^*,T)/\tau(f = 0,T)$ increases when temperature is reduced. This is consistent with the presence of increasingly cooperative relaxation mechanisms in the presence of pinned spins. While the SPM without pinning has "strong" glass scaling, $\tau(f = 0) \sim e^{3/T}$, we find that $\tau(f^*)$ increases in a super-Arrhenius (fragile) fashion. This indicates that the relaxation mechanism for the system near f^* is different from the bulk mechanism at $f = 0$, presumably because the frozen spins act to frustrate relaxation of the mobile ones.

We expect many of the results shown for the SPM to be quite generic in glassy systems. Certainly, the behavior in the TPM is similar. Figure 2 shows data for $C(t)$ and $\chi_4(t)$ in the TPM at the representative temperature $\beta = 3$. As before, $C(t)$ exhibits a plateau at long times which increases with f, while the static susceptibility χ_4 is maximal at some $f = f^*$. Consistent with the SPM, we also find that f^* decreases at low temperature, that the maximum of the static susceptibilities increase, and that the time scales at f^* increase. These results resemble

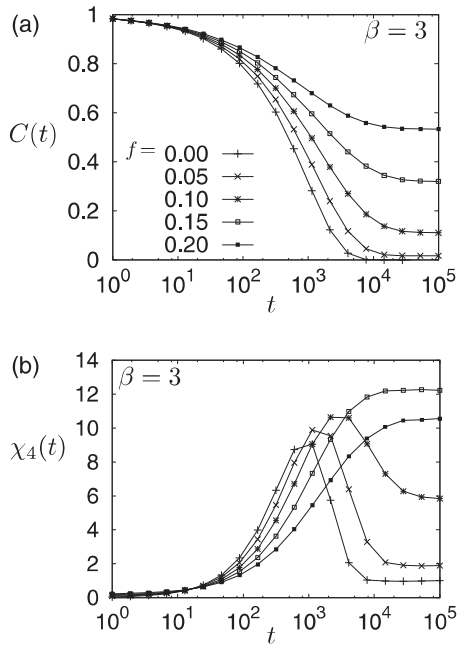

FIG. 2. Effects of pinning in the TPM at $\beta = 3$. (a) Time-dependent correlation function. (b) Time-dependent four-point susceptibility.

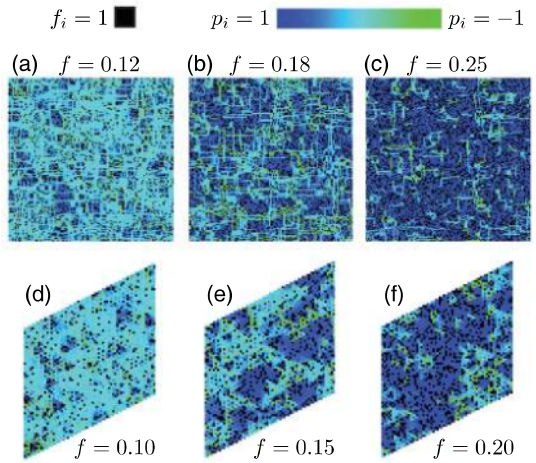

FIG. 3. (Color online) Snapshots of the propensities p_i in the long-time limit. (a)–(c) SPM at $\beta = 3$, varying f. At this temperature $f^* \approx 0.18$. (d)–(f) TPM at $\beta = 3$ for which $f^* \approx 0.15$. Pinned spins are black while unpinned spins are color coded with dark blue (dark gray) for $p_i \approx 1$, and pale blue or green (light gray) for $p_i \approx 0$ and $p_i \approx -1$, respectively. On increasing f, the spins become polarized so that $p_i \approx 1$ in most cases. The correlations associated with the propensity are strongest near f^*, consistent with χ_4 being maximal.

strongly the ones shown in Fig. 1, and are therefore not shown, for brevity. However, the f dependence of the relaxation time τ is weaker in the TPM than in the SPM: The ratio $\tau_{\max}/\tau_0$ does increase systematically on decreasing temperature but it takes values in the range 1–4 while τ_0 varies over nearly four orders of magnitude.

We emphasize that all of the results presented in this article are obtained in large systems and we have checked that they are free from finite-size effects. (This is discussed further in Sec. IV C below.) We find that susceptibilities and relaxation times have maxima at f^*, but the maximum values remain finite even when the thermodynamic limit is taken, $V \to \infty$. Thus, there are no diverging correlation times or correlation lengths in this system for any finite f or T, nor is there any phase transition. However, we find that correlation times and susceptibilities have sharp maxima along a line $f^*(T)$ in the (f,T) phase diagram.

IV. SCALING OF LENGTHS

We have shown that varying f in the SPM and TPM reveals crossovers at f^*, associated with maxima in susceptibilities and in relaxation times. We now discuss how these features can be related to correlation lengths in these systems. In particular, we focus on the scaling of these length scales at low temperatures.

A. Visualisation of spatial correlations

It is instructive to visualize the spatial fluctuations that appear as a result of the random pinning. To this end, we consider the dynamic propensity [42,43]. (Compared to visualising the autocorrelations a_i directly, the propensity provides continuous functions rather than binary ones, and this yields images that better differentiate between regions where relaxation is frustrated by the frozen spins and those where relaxation can occur.)

To calculate the propensity, we take a single representative reference configuration, $\boldsymbol{s}^{\mathrm{A}}$, in which a specific set of spins are frozen, and we run several long MC trajectories starting from it. We calculate the autocorrelation $a_i(t) = s_i(t)s_i(0)$ for each unfrozen spin in each trajectory and we average over the trajectories to obtain the (site-dependent) propensities $p_i(t) = \overline{a_i(t)}$. For large times these propensities approach limiting values, $p_i = p_i(t \to \infty)$, which depend on the reference configuration $\boldsymbol{s}^{\mathrm{A}}$ but not on the time t. The propensities are therefore static on-site quantities characterizing the degree of freezing of spin i for a given realization of the random pinning and a given reference configuration.

Representative results are shown in Fig. 3, where pinned spins are shown in black, and a blue-green color coding describes the propensity. Sites for which the pinned spins cause the configuration to remain near its initial state have $p_i \approx 1$ (dark blue) while those where the pinned spins have little effect have $p_i = 0$ (light blue). If the frozen spins cause s_i to become polarized in the opposite direction to s_i^{A}, one finds $p_i < 0$ (green).

At $f = 0$ then $p_i = 0$ for all i and the system is homogeneous. As f starts to increase (left panel), then the system acquires regions where the spins become polarized and cannot relax any more (colored dark blue in Fig. 3). This seems to occur in small, isolated regions whose size increases with f. For $f \approx f^*$ (middle panel), these polarized regions percolate throughout the system and spatial fluctuations of the propensity occur over a large length scale. This yields snapshots where large regions are strongly polarized while others are unaffected by the pinning. Finally, as f increases further above f^* (right panel), most spins are strongly pinned, and only few

small regions exist where motion remains possible. In this regime, the system is strongly localized near the reference configuration.

An important observation is that the length scales associated with these correlations observed near f^* are much longer than the typical distance $f^{-1/2}$ between pinned spins. This is apparent in Fig. 3, because the colored domains are clearly much larger than the spacing between (black) pinned sites. In other words, each correlated region in these images contain very many pinned spins. These observations will be quantified below in Sec. IV C.

The qualitative description of these images is strongly reminiscent of observations made in dynamic heterogeneity studies [10], except that time has now been replaced by the fraction of pinned spins. The images in Fig. 3 suggest that a similar behavior is found in both square and triangular models but that the specific features of the models will be reflected in the form of the correlation functions. For example, the SPM is characterized by strongly anisotropic correlations, while correlations appear more isotropic for the TPM, although they do have an underlying fractal structure. These observations once again echo previous studies of the dynamic heterogeneity in these models [16].

B. SPM: "Bulk" scaling at $f = 0$

To analyze length scales and their scaling in the SPM, it is useful to start by considering static correlations for the "bulk" at $f = 0$. As discussed in Sec. II, the first nontrivial correlations involve four spins arranged at the edges of a rectangle of size $x \times y$. It is clear from Eq. (3) that lines $xy =$ const. are contours of the static four-point function $g_s(x,y)$; that is, the four-spin correlations are strongly anisotropic, which leads to unusual scaling behavior at low temperature ($c \to 0$). For example, one may measure correlations at a fixed finite angle θ to the lattice axes (with $\theta \neq 0, \pi/2$, etc.), in which case,

$$g_s(x,y) \simeq G_{so}(r\sqrt{c},\theta), \tag{11}$$

with $x = r\cos\theta$ and $y = r\sin\theta$, as usual. [Explicitly, $G_{so}(u,\theta) = \mathrm{e}^{-u^2 \sin 2\theta}$.] Since the scaling variable is $u = r\sqrt{c}$, the correlation length away from the lattice axes scales as $1/\sqrt{c}$. (Throughout this section we use the symbol G for scaling functions, with the approximate equalities valid on taking $c \to 0$ with the arguments of G held constant.)

However, a larger static correlation length in this system is revealed by measuring $g_s(x,y)$ along the axes of the square lattice. For fixed y (of order unity) and varying the temperature, one gets

$$g_s(x,y) \simeq G_{sa}(xc,y), \tag{12}$$

indicating a correlation length $\xi \sim c^{-1}$, measured along the lattice axes. [Explicitly, $G_{sa}(u,y) = e^{-2yu}$].

At low temperatures, one may also show that the circular average of $g_s(x,y)$ is dominated by contributions from near the axis and so it also decays on a length scale $\xi \sim c^{-1}$, as $g_s(r) \simeq r^{-1} G_{sr}(rc)$, which may be rewritten as

$$g_s(r) \simeq c\, G_{sc}(rc), \tag{13}$$

that is, the effect of the circular average is to pick up the longest of the two length scales that appear in $g_s(r)$.

C. SPM: Real-space scaling at $f = f^*$

In Fig. 4, we show the behavior of $g_{4,ij}$ and X_{ij} for $f = f^*$ and a representative temperature $\beta = 3$. We compare these correlations with the behavior of $g_{4,ij}(t)$ measured at $f = 0$ and $t = \tau$, for the same temperature. In all cases, the correlations seem to operate over a similar length scale (the same linear scale is used for all panels). The correlation functions are all strongly anisotropic, although we observe slightly different angular dependencies in each case.

The dominance of a single length scale in this problem may be seen from Fig. 5 where we show circular averages of these correlation functions, plotted as a function of the scaling variable rc. It was shown in Ref. [16] that dynamical four-point correlations at $f = 0$ and $t = \tau$ collapse as a function of this

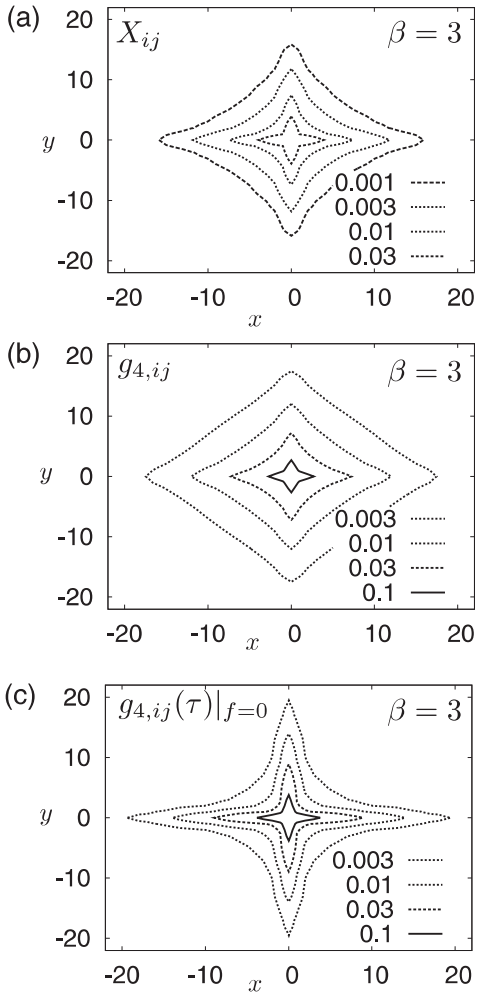

FIG. 4. Real-space correlations in the SPM. (a) The correlation function X_{ij} evaluated at $f = f^*$, in the long-time limit. The coordinates x and y give the position of spin j relative to spin i. (b) The four-point susceptibility $g_{4,ij}$ at $f = f^*$ and long times. (c) The four-point susceptibility at $f = 0$, evaluated at the bulk relaxation time τ. The scales are the same in all plots, indicating that all correlations operate over similar length scales.

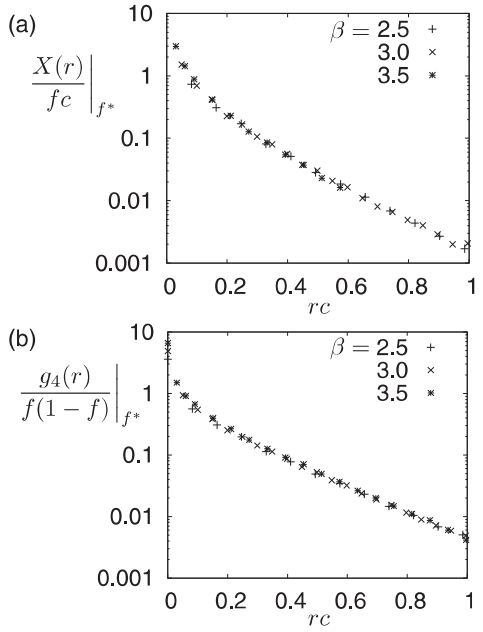

FIG. 5. Circular averaged correlation functions in the SPM evaluated at $f = f^*$ and plotted to illustrate their scaling with temperature. (a) Circular average of X_{ij}. (b) Circular average of $g_{4,ij}$. In both cases the relevant length scales scale as $\xi \sim c^{-1}$. At the lower temperatures we show data points are only for those r and β where numerical uncertainties are smaller than or comparable to symbol sizes.

scaling variable. Here we show that the same behavior holds for X_{ij} and $g_{4,ij}$ evaluated at f^*.

To describe the scaling behavior of correlation functions near f^* in the SPM, we make an ansatz for the circular averaged three-point function $X(r)$:

$$X(r)|_{f^*} \approx cf^* G_X(rc). \tag{14}$$

The choice of scaling variable rc indicates that the dominant correlation length in the system scales as $\xi \sim c^{-1}$. To understand the prefactor cf^*, note that the ratio X_{ij}/f quantifies the effect of freezing spin j on the autocorrelation function at site i. Thus, if each frozen spin has an $O(1)$ effect then one would expect $X(r) \approx fG(r)$, which explains the presence of f^* as a prefactor in Eq. (14). The extra prefactor of c in Eq. (14) has two possible interpretations, which are hard to discriminate on the basis of our numerical results. First, if the correlation function $X(x,y)$ is largest near the lattice axis, and if these on-axis correlations are $O(1)$ and dominate the circular average then one arrives at $X(r)/f \approx c\, G_X(r)$, as in the case of the static function $g_s(r)$. However, a second explanation could be the presence of off-axis correlations of strength $O(c)$, which would lead to the same prefactor c in Eq. (14).

Our ansatz for the low-temperature scaling of g_4 is

$$g_4(r)|_{f^*} \approx f^*(1-f^*)G_4(rc). \tag{15}$$

Again, the scaling variable rc indicates that the correlation length scales as $\xi \sim c^{-1}$. In Fig. 5, we plot $g_4/[f^*(1-f^*)]$ as a function of the scaled variable rc, a procedure which nicely collapses our data. The prefactor $(1-f^*)$ is irrelevant for the purpose of scaling in the low-temperature limit. However, it is natural from a physical point of view because $g_{4,ii} \propto (1-f)$, and we do find that it improves the data collapse in the studied range of temperatures. The physical interpretation of the prefactor f^* in Eq. (15) is not immediately clear. We note that Eqs. (14) and (15) are together consistent with Eq. (10), which holds if the correlations of the a_i are directly attributable to individual frozen spins f_j. More support for this can be obtained through a direct numerical evaluation of the right-hand side of Eq. (10) which has the same dependence on ij as $g_{4,ij}$, but is smaller by a factor close to 5, independently of the temperature. As a result, χ_4 and its bound $\Delta\chi_4$ scale in the same way, but differ by a prefactor.

To conclude, we have shown robust evidence that $g_{4,ij}$ and X_{ij} in the SPM are both controlled by the same length scale $\xi \sim (1/c)$. The scaling of the prefactors in these correlations is less clear, but Eqs. (14) and (15) are consistent with our numerical data. Assuming that these results do hold, we arrive at the following scaling behaviors for the susceptibilities:

$$\left.\frac{\partial q}{\partial f}\right|_{f^*} \sim c^{-1}, \qquad \chi_4|_{f^*} \sim \Delta\chi_4|_{f^*} \sim c^{-2} f^*. \tag{16}$$

We recall that dynamical correlations $g_4(r,t)|_{f=0}$ at $t = \tau$ are controlled by the same length scale $\xi \sim (1/c)$, but that $\chi_4(t=\tau)|_{f=0} \sim c^{-1}$ due to the strong anisotropy of the correlation function. Combined with the super-Arrhenius growth of the relaxation time shown in Fig. 1(f), this difference in the scaling of χ_4 emphasizes that the relaxation near f^* is qualitatively different from bulk relaxation at $f = 0$, even if the same length scale appears in both cases. In particular, the susceptibility χ_4 at f^* grows more quickly on cooling than the bulk χ_4, consistent with the observation that relaxation is slower and more cooperative. In this respect increasing f^* is similar to reducing the temperature. However, in contrast to decreasing T, there is no evidence for an increasing length scale as f is increased.

We commented above that finite-size effects are small in our data. To illustrate this, we note from Fig. 4 that the range of correlations in the SPM at $\beta = 3$ is of the order of 20 lattice spacings: We used a lattice of linear size $L = 128$ for simulations at that temperature. For the lowest temperatures considered, we used lattices of size $L = 256$, again much bigger than the range of spatial correlations. In Fig. 5 we show that spatial correlations decay exponentially, and we do not find any evidence for weak long-ranged correlations that might contribute significantly to the susceptibilities χ_4 and $\partial q/\partial f$. In fact, the results we show for χ_4 in Figs. 1 and 2 were obtained by summing $g_{4,ij}$ over j as in (5): We restrict the sum to sites j within a range r of site i, ensuring that the sum has converged to its large-r value but choosing r to minimize the numerical uncertainty in χ_4.

D. TPM: Real-space scaling at $f = f^*$

For the triangular plaquette model, the isotropic images shown in Fig. 3 lead us to compute circularly averaged correlation functions directly. The results are presented in Fig. 6, showing scaling with temperature. We find that our data are most consistent with

$$X(r)|_{f^*} \approx cf^* G_{XT}(rc), \tag{17}$$

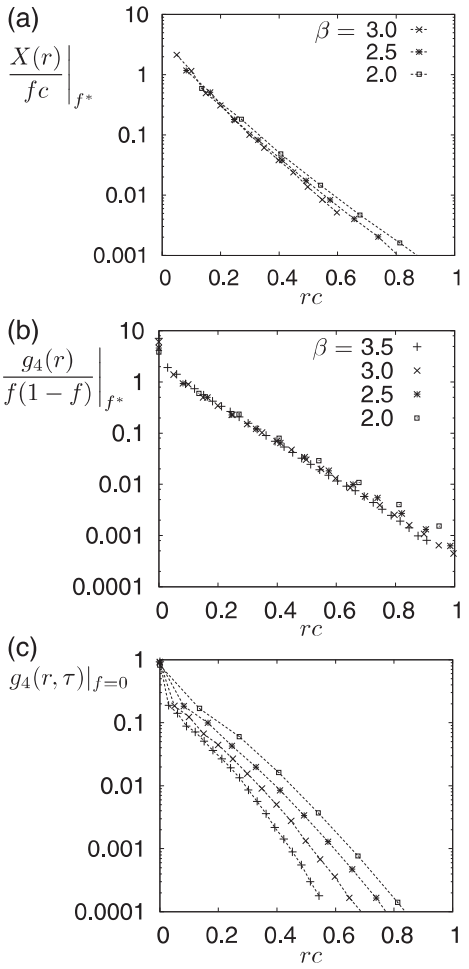

FIG. 6. Circular-averaged correlations in the TPM. (a) Circular average of X_{ij} at f^*, showing a length scale $\xi \sim c^{-1}$. (b) Circular average of $g_{4,ij}$ at f^*, showing a similar length scale $\xi \sim c^{-1}$. (c) Circular average of $g_{4,ij}(t)$ evaluated at $f = 0$ and $t = \tau$. This correlation function clearly has a different scaling to those evaluated at f^*: It was shown in [17] that $\xi \sim c^{-1/d_f}$ in this case.

and

$$g_4(r)|_{f^*} \approx f^*(1-f^*)G_{4T}(rc). \tag{18}$$

The most striking feature of Eqs. (17) and (18) is that the scaling variable rc is the same as that found in the SPM. This suggests that correlations at f^* extend over a length which scales as $\xi \sim 1/c$. This is surprising because the point-to-set length for the TPM at $f = 0$ does not scale as c^{-1}, nor does the dynamic correlation length. For dynamical correlations at $f = 0$ and $t = \tau$ then it is known [17] that $g_4(r,\tau)|_{f=0} \approx G_{4T}(rc^{1/d_f})$, such that both static and dynamic lengths scale as $\xi(f = 0) \sim c^{-1/d_f} \sim c^{-0.631}$. In Fig. 6(c), we show that these two scaling forms can be clearly differentiated over the temperature range shown, since $g_4(r)|_{f=0}$ does not collapse as a function of rc, as expected. It is therefore clear that a new length scale $\xi \sim c^{-1}$ appears in the TPM near $f = f^*$, which is longer than any static or dynamic correlation length found previously for the bulk at $f = 0$.

As in the SPM, the physical interpretation of the scaling prefactors in Eqs. (17) and (18) is not clear. The scaling laws we have proposed indicate that the bound $\Delta\chi_4$ scales in the same way as χ_4, although $\Delta\chi_4$ is significantly smaller than χ_4 in the TPM. We also note that while the scaling forms in Eqs. (17) and (18) in the TPM are the same as in Eqs. (14) and (15) in the SPM, we do not see any *a priori* reason for this result. In particular, the spatial structure of the correlations are quite different in both cases.

While the appearance of a new length scale near f^* makes the TPM different from the SPM, we emphasize that the relaxation mechanism changes qualitatively near f^* in both models. In the SPM, this appears as a larger relaxation time and a larger susceptibility without any increase in the length; in the TPM the length scale, time scale and susceptibilities are all different from their values at $f = 0$.

V. SQUARE PLAQUETTE MODEL: WEAK AND STRONG PINNING

We have discussed the scaling of length and time scales at f^*, as temperature is reduced. In this section, we consider how f^* depends on temperature. We focus on the SPM for which analytic calculations provide useful insight.

A. Small-f limit

We concentrate on the behavior of the correlation function X_{ij}. We define a parameter μ by $f = (1 + e^{\mu})^{-1}$ so that the limit of small f is equivalent to a limit of small $e^{-\mu}$. The correlation function X_{ij} has a series expansion in powers of $e^{-\mu}$ given by

$$X_{ij} = \frac{1}{Z_f}\left[\langle a_i f_j\rangle_0 + e^{-\mu}\sum_k \langle a_i f_j\rangle_k + e^{-2\mu}\sum_{k<l}\langle a_i f_j\rangle_{kl} + O(e^{-3\mu})\right] - qf(1-f), \tag{19}$$

where $Z_f = (1 + e^{-\mu})^V$ and $\langle\cdots\rangle_{kl\ldots}$ is an average in a system where spins $(k,l,\ldots)$ are pinned and all other spins are mobile (unpinned). For details, see the Appendix, particularly Eq. (A4). The factor of q in Eq. (19) must be obtained by a separate series expansion over f.

Assuming $i \neq j$, symmetries of the SPM imply that the first nonzero term in the expansion is at third order,

$$e^{-3\mu}\sum_{k<l<m}\langle a_i f_j\rangle_{klm}. \tag{20}$$

The factor f_j means that the average is zero unless j is equal to one of k, l, or m. As shown in Fig. 7, the correlations may be calculated in a diagrammatic expansion. Spin i is shown as a white circle and has a fixed position. Spin j is shown as a gray circle: Its position is fixed, and we also have the constraint that one of the frozen spins k, l, or m coincides with j. Equation (19) shows that we must sum over the positions of the remaining frozen spins: These spins are shown as black circles. To evaluate the contribution of each diagram to X_{ij}, we use Eq. (A5) which shows how to evaluate expectation values in the presence of a fixed set of frozen spins. For the SPM, $\langle a_i f_j\rangle_{klm}$ is nonzero only if spins $iklm$ lie on the four vertices

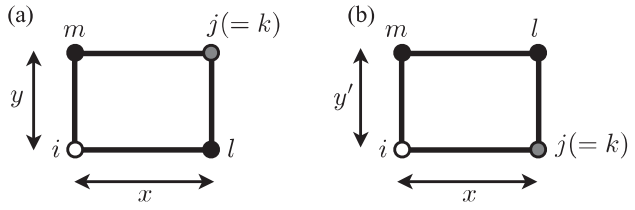

FIG. 7. Two diagrams representing contributions to X_{ij} in the SPM, at order f^3. The white circle represents spin i, the gray circle spin j, and the positions of spins klm are to be summed, subject to the constraint that j is equal to one of klm. (a) Leading contribution to $X(x,y)$, assuming $x,y > 0$. (b) Leading contribution to $X(x,0)$: Summing over the positions of spins l and m corresponds to a sum over the dimension y'.

of a rectangle. If the rectangle is of size $x \times y$ then Eq. (A5) yields $\langle a_i f_j \rangle_{klm} = \tanh(\beta/2)^{2xy}$. [The denominator in (A5) has a trivial value 2^{-3} in this case, because all configurations of the frozen spins are equally likely and they all have equivalent effects on spin i.]

The leading order behavior of X_{ij} stems from two distinct cases, as shown in Fig. 7. If spins i and j are in the same row of the square lattice, with spacing x, then we fix $k = j$ and we sum over all sites l and m such that the sites $iklm$ form a rectangle. For a rectangle of size $x \times y'$ then Eq. (A5) yields $\langle a_i f_j \rangle_{klm} = \tanh(\beta/2)^{2xy'}$. Summing over the positions of spins l and m, one obtains a geometric series and the result is, for $x \neq 0$,

$$X(x,0) = f^3 \frac{\tanh(\beta/2)^{2|x|}}{1 - \tanh(\beta/2)^{2|x|}} + O(f^4), \qquad (21)$$

where we have defined $X(x,y) = X_{ij}$, evaluated for spins i and j that are separated by a vector (x,y). A similar analysis applies if spins i and j are in the same column of the lattice, yielding $X(0,y) = X(y,0)$.

However, if spins i and j are in different rows and columns then we fix $l = j$ and we sum over sites k and m such that sites $iklm$ still form a rectangle. There is only one choice for k and m in this case, as shown in Fig. 7(b). If the vector from site i to site j is (x,y) then the resulting rectangle is $x \times y$ in size and, again, $\langle a_i f_j \rangle_{klm} = \tanh(\beta/2)^{2xy}$ so that, for $x,y \neq 0$,

$$X(x,y) = f^3 \tanh(\beta/2)^{2|xy|} + O(f^4). \qquad (22)$$

Collecting all these results and summing over the volume, Eq. (8), one finally obtains the leading order behavior of the three-point susceptibility, namely,

$$\frac{\partial q}{\partial f} = 12 A_c(T) f^2 + O(f^3), \qquad (23)$$

where

$$A_c(T) = \sum_{x=1}^{\infty} \frac{\tanh(\beta/2)^{2x}}{1 - \tanh(\beta/2)^{2x}} \simeq \frac{e^\beta}{4}[\beta + O(1)]. \qquad (24)$$

The final approximate equality holds for small c (i.e., at low temperature) and follows because $\sum_k (1-\delta)^k/(1-(1-\delta)^k) \approx (1/\delta)[\log(1/\delta) + O(1)]$ as $\delta \to 0$. In Fig. 8(a) we show that the result in Eq. (23) holds very well for small values of

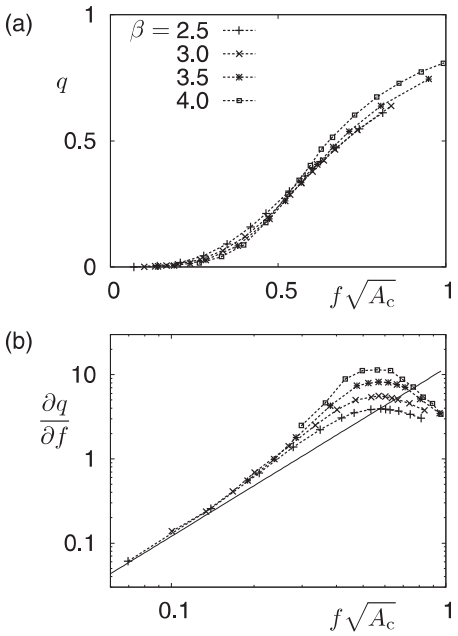

FIG. 8. Plots of q and $\partial q/\partial f$ for the SPM, as a function of the scaling variable $f\sqrt{A_c}$. (a) Plot of the overlap q indicating that $f^* \sim A_c^{-1/2}$. (b) The susceptibility $\partial q/\partial f$ is maximal near f^*. The straight line is the theoretical result (23) for the small-f limit. This approximation applies only when $f\sqrt{A_c} \ll 1$ and does not capture the peak in $\partial q/\partial f$ near f^*.

$f\sqrt{A_c}$, but breaks down for larger f, where higher-order terms in the expansion also contribute, as discussed below.

The physical interpretation of this small-f result is that adding one extra frozen spin j affects the autocorrelation a_i over an area of linear size $\xi \sim c^{-1}$, but the anisotropy of correlations imply that the correlation volume is $v \sim A_c \sim (-\ln c)/c$, much smaller than the naive assumption $v \sim \xi^2 \sim 1/c^2$. The strength of the response on adding the frozen spin is small (proportional to f^2) but the length scale controlling X_{ij} is large and independent of f as $f \to 0$, and the sum in Eq. (8) is dominated by correlations close to the lattice axes.

Using Eq. (23), it is then easy to integrate $\partial q/\partial f$ to obtain the low-f behavior of the overlap,

$$q = 4 A_c f^3 + O(f^4). \qquad (25)$$

It is interesting to remark that $A_c = \sum_{xy(\geqslant 0)} g_s(x,y)^2$, which highlights the fact that in the limit where the randomly frozen spins are dilute, the static overlap and susceptibilities simply capture the most trivial behavior of the bulk system. In a supercooled liquid where two-body correlations do not vanish, one would expect the overlap to be proportional to f for small f, with a prefactor directly given by the pair correlation function [see Eqs. (19) and (A8)]. It is only by going beyond the leading order in f one reveals the relevant higher-order correlations responsible for amorphous order [11,25].

B. SPM: Behavior near $f = f^*$

To analyze the behavior near $f = f^*$, we now consider higher-order terms in the expansion over f. In Fig. 9, we show

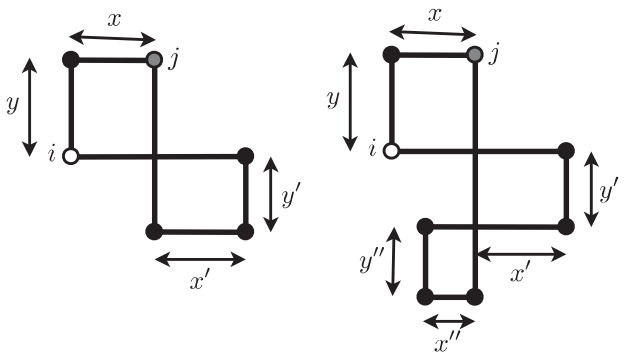

FIG. 9. Two representative diagrams that contribute to X_{ij} in the SPM, at order f^5 (left) and f^7 (right). The dimensions x and y are fixed by the positions of spins i and j while the primed dimensions are to be summed over. These sums yield factors of A_c (left) and A_c^2 (right) in the contributions of these diagrams to X_{ij}.

two further contributions to X_{ij}, in the case where i and j are not in the same row or column. These contributions appear at order $e^{-5\mu}$ and $e^{-7\mu}$ in Eq. (19), respectively. For these diagrams, Eq. (A5) yields $\langle a_i f_j \rangle_{kl\ldots} = \tanh(\beta/2)^{2\mathcal{A}}$ where $\mathcal{A}$ is the total area of the rectangular regions enclosed by the solid lines in the diagrams. [The denominator in Eq. (A5) is again trivial for these diagrams, due to symmetries of the SPM.] Summing over the positions of the frozen spins yields a factor of A_c for each rectangle, except for the rectangle whose location is fixed by the positions of i and j. These two diagrams therefore contribute to X_{ij} as $f^3(f^2A_c)\tanh(\beta/2)^{2xy}$ and $f^3(f^2A_c)^2\tanh(\beta/2)^{2xy}$, respectively. Of course, there are various other contributions at these orders that scale in the same way. Constructing higher-order diagrams similar to those in Fig. 9, one may identify a series of positive terms which are all proportional to powers of f^2A_c. For small c, we expect these to be the largest terms at each order. These considerations clearly motivate the use of $f\sqrt{A_c}$ as a scaling variable for this expansion. Of course, if f^2A_c is not a small number, then the leading terms in the small-f expansion do not give a good approximation to the correlation function.

In Fig. 8 we plot q and $\partial q/\partial f$ as a function of the scaling variable $f\sqrt{A_c(T)}$. We find that the crossover f^*, which corresponds to the maximum observed for $\partial q/\partial f$, does indeed scale as $A_c^{-1/2}$, so that finally

$$f^*(T) \approx \sqrt{\frac{-\ln c}{c}} \sim \sqrt{T}\exp\left(-\frac{1}{2T}\right). \qquad (26)$$

This result shows that the "localization" crossover at f^* occurs along a line $f^*(T)$ in the (f,T) phase diagram, with $f^* \to 0$ as $T \to 0$.

In addition, the numerical data indicate that results from the small-f limit such as Eq. (23) are applicable only when $f\sqrt{A_c} \ll 1$ and break down for $f \simeq f^*$. As suggested above, this strongly suggests that the maxima in $\partial q/\partial f$ and χ_4 have their origin in nontrivial "many-body" effects that are not captured by the low-order expansion about the dilute limit.

Physically, the interpretation is that the relaxation mechanism near f^* is qualitatively different from the bulk relaxation at $f = 0$. Perturbation theory in f is not sufficient to capture this new mechanism: A nonperturbative approach would be necessary to make further analytic progress, presumably by summing infinite subsets of diagrams in the expansion of correlation functions. In this model, $f^* \to 0$ when $T \to 0$, indicating that the regime where perturbation theory is valid becomes vanishingly small near the glass transition of the model (which takes place at $T = 0$).

VI. DISCUSSION

We have studied the effect of random pinning in the context of two finite dimensional spin models with plaquette interactions. By increasing the fraction f of pinned spins at a fixed low temperature, we have discovered the existence of a temperature-dependent crossover between bulklike relaxation at small $f < f^*(T)$, and a nearly localized amorphous state at large $f > f^*(T)$. The study of static correlation functions and susceptibilities in the presence of random pinning directly reveals the existence of growing amorphous order on cooling. This growth appears through the large length scales that can be measured by X_{ij} and $g_{4,ij}$, and by the decreasing values $f^*(T)$ required to keep the system localized in a single state at lower temperature. Moreover, these measurements do not require *a priori* knowledge of the specific type of order that sets in at low temperature. These results therefore demonstrate that the main objective underlying the measurement of point-to-set correlation functions is fulfilled in plaquette models.

The length scales that we measure show scaling behavior at low temperatures. We have emphasized that while low-order terms in the expansion over f are related to static correlation functions of the bulk system at $f = 0$, the length and time scales that we observe near $f = f^*$ are related to nonperturbative effects, and analytic calculations of length scales in that regime would seem to require a new approach beyond those given here.

Similarly, we have shown that length and time scales near f^* in the plaquette models are not related in the same way as they are at $f = 0$. Increasing f in the SPM, we found an increasing time scale and a growing susceptibility, but without any increasing length scale. In the TPM, the length scale increases as f is increased but the change in time scale is very mild, in contrast to the strong dependence observed at $f = 0$ for this model.

We have also emphasized that although static and dynamic correlations are strongly enhanced near f^* as compared to the bulk, length and time scales are finite at f^*, after taking the thermodynamic limit at any nonzero temperature. This implies that random pinning does not induce any kind of phase transition in plaquette models. It is perhaps unsurprising that these models do not exhibit an ideal glass transition in the (f,T) phase diagram, since no transition occurs at finite temperature in the bulk at $f = 0$ either. However, the sharp crossovers we have revealed in plaquette models represent nontrivial new results, because they have no counterparts in the bulk systems at $f = 0$.

Given that neither mode-coupling theory nor RFOT theory represent accurate descriptions of plaquette models in the bulk, we do not expect these approaches to account for the effect of random pinning either. Thus, we argue that the results obtained within plaquette models provide a useful alternative reference point for interpreting simulation data for more realistic models

of supercooled liquids. In particular, the absence of any phase transition at f^* indicates that such transitions may not be generic in glassy systems with pinning.

In this respect, it is instructive to compare the results we find here with the predictions of RFOT theory [12]. A central quantity in this theory is the configurational entropy, which measures the diversity of long-lived metastable states. Assuming that RFOT applies in supercooled liquids, results for model systems and renormalization group calculations [12] indicate that the configurational entropy density s_c is well represented by

$$s_c(T,f) \approx s_c(T,0) - fY(T). \tag{27}$$

In three dimensions and above, this leads to a phase transition at $f^*(T) \approx Y(T)/s_c(T,0)$. In two dimensions, this transition is destroyed by fluctuations and becomes a crossover. Similarly, fluctuations in three-dimensional systems mean that the phase transition at f^* will occur only for low temperatures, close to the glass transition. At higher temperatures, this transition should become a crossover.

In addition, RFOT predicts that a length scale $\xi_{\rm PTS}$ grows as $s_c(f,T)$ approaches zero, and that the relaxation mechanism at finite f involves cooperative rearrangements over the length scale $\xi_{\rm PTS}$, much as in the bulk. We emphasise that s_c is related to metastable states and may not be obtained from the statistics of minima on the system's energy landscape. A precise definition of s_c in finite-dimensional systems is slightly problematic since all metastable states have finite lifetime in that case. However, one may follow the procedure of Ref. [6], as long as the time scale associated with structural relaxation is well separated from all microscopic time scales.

Turning to the plaquette models, the geometric construction of Ref. [6] indicates that s_c decreases as f increases, just as in RFOT theory. However, it is clear from Fig. 3 that even for $f > f^*$ there are sets of spins that may rearrange cooperatively, which ensures that s_c does not vanish at f^*. Thus, while s_c presumably decreases sharply near f^*, it does not drop to zero as predicted by Eq. (27). For supercooled liquids, RFOT predicts instead localization in a single state for $f > f^*$, so that if the analysis of Sec. IV were repeated for those systems then regions where cooperative motion is possible should be forbidden for $f > f^*$, and the light-colored regions shown in Fig. 3 would be completely absent. In plaquette models, the existence of such regions restores a finite configurational entropy density above f^* and the proposed phase transition is avoided. It is unclear whether such strong spatial fluctuations can be present in supercooled liquids, and whether they are properly captured by renormalization group treatments [12]. This remains an area of ongoing research [44–47].

Thus, the plaquette models illustrate that even if the detailed predictions of RFOT do not apply, systems where configurational entropy decreases on pinning can be generically expected to exhibit increased cooperativity on increasing f, accompanied by growing time scales as well as growing lengths and/or growing static susceptibilities. One may also expect crossovers that sharpen and move to small f on cooling. To this extent, the plaquette models are broadly consistent with published numerical results for particle models [11,23–25,37], although the f dependence of the relaxation time appears much weaker in the plaquette models in comparison with model liquids.

On the other hand, the most striking prediction of RFOT theory is the presence of a phase transition at finite f^*, in supercooled liquids. This transition remains to be found numerically, as the behavior for large values of f and low temperatures has not been investigated in much detail so far. At higher temperatures, the observation of a crossover between bulk relaxation and localized behavior is consistent with RFOT. However, in the absence of a phase transition, we argue that the detailed RFOT scaling predictions for length and time scales at the crossover must be tested directly in order to substantiate the theory and distinguish it from a more general picture of increasing cooperativity in the presence of pinning. Testing these scaling predictions remains a very challenging task, especially in the absence of direct measurements of the configurational entropy. We therefore conclude that while pinning particles is an interesting new method of measuring amorphous order and its growth upon cooling, it does not necessarily resolve the central problem of how to test the fundamental assumptions of RFOT theory by practical measurements. Nevertheless, we hope future studies will investigate further the effect of random pinning in supercooled liquids, especially in the relatively unexplored regime of strong pinning.

ACKNOWLEDGMENTS

We thank G. Biroli, D. Coslovich, W. Kob, and G. Tarjus for useful discussions. R.L.J. thanks the Engineering and Physical Sciences Research Council (UK) for financial support through Grant No. EP/I003797/1.

APPENDIX: CORRELATIONS IN SYSTEMS WITH RANDOM PINNING

In this appendix, we discuss some general results for spin systems in the presence of pinning.

1. Ensemble dependence of $\chi_4(t)$

In the systems considered here, the set of frozen spins $\boldsymbol{f}$ remains constant as the dynamics proceeds. This results in ensemble-dependent susceptibilities [38–40], such as

$$\chi_4(t) = \chi_{4F}(t) + \Delta\chi_4(t), \tag{A1}$$

where $\chi_{4F}(t) = [(1-f)V]^{-1}\langle \delta\hat{Q}(t)^2\rangle_f$ is evaluated in a "restricted" ensemble with a fixed number of frozen spins. Analysis of such ensemble dependence can be useful for understanding how the time-independent variables (the frozen spins in this case) influence the time-dependent ones.

The difference term $\Delta\chi_4(t)$ may be derived as in Ref. [40] or equivalently following Ref. [48]. We write $\hat{Q} - \langle\hat{Q}\rangle = (\hat{Q} - \langle\hat{Q}\rangle_f) + (\langle\hat{Q}\rangle_f - \langle\hat{Q}\rangle)$ where $\langle\cdots\rangle_f$ is an average with fixed $\hat{N}_{\rm f}$, as above. Substituting into Eq. (5), we note that if the restricted ensemble has $\hat{N}_{\rm f} \approx fV$ frozen spins then $\langle\hat{Q}\rangle_f - \langle\hat{Q}\rangle \approx V^{-1}(\partial\langle\hat{Q}\rangle/\partial f)(\hat{N}_{\rm f} - fV)$ which gives $\langle\delta\hat{Q}(t)^2\rangle = \langle\delta\hat{Q}(t)^2\rangle_f + V^{-2}(\partial\langle\hat{Q}\rangle/\partial f)^2\langle(\delta\hat{N}_{\rm f})^2\rangle$ (the equality is exact in the limit of large system size V, since the fluctuations of $\hat{N}_{\rm f}$ are small in that case). Noting that $\langle(\delta\hat{N}_{\rm f})^2\rangle = Vf(1-f)$ and $\partial\langle\hat{Q}\rangle/\partial f = V[(1-f)\partial C(t)/\partial f - C(t)]$ then the result (9) follows.

Since $\chi_{4F}(t)$ and $\Delta\chi_4(t)$ are both non-negative then $\chi_4(t) \geqslant \Delta\chi_4(t)$. If this bound is saturated, this means that the correlations between the a_i are directly attributable to the influence of individual f_j. In particular, a sufficient condition for $\chi_4(t) = \Delta\chi_4(t)$ is that for a fixed choice $\boldsymbol{f}$ of frozen spins, the autocorrelations a_i are all independent and respond linearly to the f_j, so that $\langle a_i(t)\rangle_f = \langle a_i(t)\rangle_0 + \sum_k f_k U_{ik}(t)$ where $U_{ik}(t) = X_{ik}(t)/[f(1-f)]$ is assumed independent of f. Physically, this condition means that the site-to-site fluctuations of the a_i depend only on the frozen spins, and the effect of each frozen spin is independent.

In addition, independence of the $\langle a_i\rangle_f$ means that $\langle a_i a_j\rangle_f = \langle a_i\rangle_f\langle a_j\rangle_f$. Following Ref. [41] we use an overbar to indicate the average over $\boldsymbol{f}$, so the definition of the four-point function is $g_{4,ij} = \overline{\langle a_i a_j\rangle_f} - \overline{\langle a_i\rangle_f}^2$. Hence, $g_{4,ij} = \sum_{kk'}[\overline{f_k f_{k'}} - f^2]U_{ik}U_{jk'}$, and since the frozen spins are chosen independently one has $\overline{f_k f_{k'}} - f^2 = f(1-f)\delta_{kk'}$. The resulting expression for $g_{4,ij}$ is given in Eq. (10) of the main text, where $g_{4,ij}$ appears as a convolution of X_{ij} with itself.

We note that for Ising spin variables s_i, it is not possible to satisfy $\langle a_i a_j\rangle_f = \langle a_i\rangle\langle a_j\rangle_f$ in the case $i = j$. However, assuming that χ_4 is dominated by collective behavior and not single-site fluctuations, one still expects Eq. (10) to hold as an approximate equality if the a_i are primarily determined by a linear response to the f_i.

2. Long-time limit

As discussed in Sec. III, long-time limits of correlation functions in systems with pinned spins are static (thermodynamic) quantities and can be calculated within equilibrium statistical mechanics. The analysis is similar to that of Krakoviack [41] for particle systems.

We write spin configurations as $\boldsymbol{s} = (s_1, \ldots, s_V)$ and choices of frozen spins as $\boldsymbol{f} = (f_1, \ldots, f_V)$. The distribution of the initial (reference) configuration $\boldsymbol{s}^{\rm A}$ is $P_1(\boldsymbol{s}^{\rm A}) = {\rm e}^{-\beta E(\boldsymbol{s}^{\rm A})}/Z_1$ where $E(\boldsymbol{s}^{\rm A})$ is the energy of configuration $\boldsymbol{s}^{\rm A}$ and the partition function Z_1 enforces normalization. The f_i are all independent with $\langle f_i\rangle = f$ and so their distribution is $P_{\rm f}(\boldsymbol{f}) = e^{-\mu\sum_i f_i}/Z_{\rm f}$ where μ is defined through $f = (1+{\rm e}^{\mu})^{-1}$ and $Z_{\rm f}$ is a normalization constant. We denote the number of frozen spins by $\hat{N}_{\rm f} = \sum_i f_i$, noting that $\hat{N}_{\rm f} + \hat{N}_{\rm m} = V$.

In the long-time limit, and for fixed $\boldsymbol{s}^{\rm A}$ and $\boldsymbol{f}$, the final configuration $\boldsymbol{s}^{\rm B}$ has probability distribution,

$$P_2(\boldsymbol{s}^{\rm B}|\boldsymbol{f},\boldsymbol{s}^{\rm A}) = \frac{1}{Z_{\rm B}(\boldsymbol{f},\boldsymbol{s}^{\rm A})} e^{-\beta E(\boldsymbol{s}^{\rm B})} \prod_i \left[(1-f_i) + f_i\delta_{s_i^{\rm A},s_i^{\rm B}}\right], \tag{A2}$$

where $Z_{\rm B}(\boldsymbol{f},\boldsymbol{s}^{\rm A})$ is a normalization factor, defined so that $\sum_{\boldsymbol{s}^{\rm B}} P_2(\boldsymbol{s}^{\rm B}|\boldsymbol{f},\boldsymbol{s}^{\rm A}) = 1$. Thus, in the long-time limit, averages $\langle\cdots\rangle$ are taken with respect to the distribution,

$$P(\boldsymbol{f},\boldsymbol{s}^{\rm A},\boldsymbol{s}^{\rm B}) = P_{\rm f}(\boldsymbol{f})P_1(\boldsymbol{s}^{\rm A})P_2(\boldsymbol{s}^{\rm B}|\boldsymbol{f},\boldsymbol{s}^{\rm A}). \tag{A3}$$

It may be shown that this distribution is invariant under $\boldsymbol{s}^{\rm A} \leftrightarrow \boldsymbol{s}^{\rm B}$. In particular, this means that the marginal distribution of $\boldsymbol{s}^{\rm B}$ is equal to the Boltzmann distribution $P_1(\boldsymbol{s}^{\rm B})$. Physically, this means that structural averages and correlation functions are unaffected by the pinning. Long-time correlations between the f_i and the a_i may be calculated as averages with respect to the distribution (A3), identifying $a_i = (1-f_i)s_i^{\rm A}s_i^{\rm B}$.

3. Small-f limit

Correlation functions between the a_i and the f_i in the long-time limit may be calculated in an expansion about $f = 0$. The idea is simply to collect together configurations $\boldsymbol{f}$ with exactly $0,1,2,\ldots$ frozen spins. Formally, one expands $P_{\rm f}(\boldsymbol{f})$ in Eq. (A3) over $e^{-\mu}$, so that for any observable Y,

$$\langle Y\rangle = \frac{1}{Z_{\rm f}}\left[\langle Y\rangle_0 + e^{-\mu}\sum_j\langle Y\rangle_j + e^{-2\mu}\sum_{j<k}\langle Y\rangle_{jk} + \cdots\right], \tag{A4}$$

where $\langle Y\rangle_{jkl\ldots}$ is an average over configurations A and B, given that spins $jkl\ldots$ are frozen and all other spins are unfrozen. [The average $\langle Y\rangle_0$ is taken without any frozen spins, so that A and B are independent configurations from the Boltzmann distribution and averages factorize as $\langle f_1(\boldsymbol{s}^A)f_2(\boldsymbol{s}^B)\rangle_0 = \langle f_1(\boldsymbol{s}^A)\rangle_0\langle f_2(\boldsymbol{s}^B)\rangle_0$.]

To make progress, the key step is to write the individual expectation values in Eq. (A4) as correlations with respect to the distribution $P_1(\boldsymbol{s}^A)P_1(\boldsymbol{s}^B)$, in which case configurations A and B are independently chosen configurations from thermal equilibrium (at $f = 0$). We write $\langle\cdots\rangle_0$ for averages with respect to this distribution. Using Eq. (A3), the general result is

$$\langle Y\rangle_{k_1k_2\ldots k_p} = \left\langle Y|_f \cdot \frac{2^{-p}\prod_{r=1}^p\left(1 + s_{k_r}^A s_{k_r}^B\right)}{Z_B(\boldsymbol{f},\boldsymbol{s}^A)}\right\rangle_0, \tag{A5}$$

where the notation $Y|_f$ indicates that any f dependence of $Y|_f$ has been accounted for by substituting the specific set of frozen spins $k_1\ldots k_p$. For example if $Y = a_i f_j$ as in the main text then $Y|_f = a_i\sum_{r=1}^p\delta_{j,k_r}$ since $Y = 0$ unless $f_j = 1$. To obtain (A5) we used $\delta_{ss'} = \frac{1}{2}(1+ss')$ for Ising spins s, s', and we also have that

$$Z_B(\boldsymbol{f},\boldsymbol{s}^A) = 2^{-p}\left\langle\prod_{r=1}^p\left(1 + s_{k_r}^A s_{k_r}\right)\right\rangle_s, \tag{A6}$$

where the average is taken over the spins s [i.e., $\langle\cdots\rangle_s = \sum_{\boldsymbol{s}}(\cdots)e^{-E(\boldsymbol{s})/T}/Z_1$].

For example, Eq. (A4) can be used to calculate $q = \langle a_i\rangle$, leading to

$$q = \langle s_i\rangle_0^2 + e^{-\mu}\left[\sum_{j(\neq i)}\left\langle s_i^A s_i^B\frac{1 + s_j^A s_j^B}{1 + s_j^A\langle s_j\rangle_0}\right\rangle_0 - V\langle s_i\rangle_0^2\right] + O(e^{-2\mu}), \tag{A7}$$

where we used $Z_{\rm f} = (1+e^{-\mu})^V$ and we assumed that averages are translationally invariant, $\langle s_i\rangle_0 = \langle s_j\rangle_0$, etc.

If the system has inversion symmetry so that $\langle s_i\rangle_0 = 0$ then the denominator in Eq. (A7) is trivial and the average may be evaluated directly. Physically, the denominator accounts for the fact that the autocorrelation $\langle a_i\rangle_f$ depends on the state of s_i in the reference configuration $\boldsymbol{s}^A$, and the different values of s_i^A may not be equally likely. In the symmetric case, both values of s_i^A are equally likely so the denominator has a trivial value.

To make progress with the general case, note that $s_i = \pm 1$ which means that for any function $F(s)$ then $F(s) = \frac{1}{2}(1+s)f(1) + \frac{1}{2}(1-s)f(-1)$ and hence (for any x), $1/(1+xs_i) = (1-xs_i)/(1-x^2)$. The result is that

$$q = \langle s_i \rangle_0^2 + f \sum_{j(\neq i)} \frac{\langle \delta s_i \delta s_j \rangle_0^2}{1 - \langle s_j \rangle_0^2} + O(f^2). \tag{A8}$$

One may similarly show that

$$X_{ij} = f \frac{\langle \delta s_i \delta s_j \rangle_0^2}{1 - \langle s_j \rangle_0^2} + O(f^2), \tag{A9}$$

and summing over j and integrating with respect to f yields Eq. (A8), via Eq. (8).

Physically, X_{ij}/f is the change in the autocorrelation $\langle a_i \rangle$ if one restricts to an ensemble where $f_j = 1$. If the spin system has two-point correlations of range ξ then Eq. (A9) shows that pinned spins influence mobile spins over a range of at least ξ, resulting in an $O(f)$ contribution to q. Of course, if two-spin correlation functions dominate the physics then the pinning procedure is redundant since the correlations may already be measured through the spin-spin correlation function. For the spin models we consider in this paper, multispin correlations dominate the physics, and we find that X_{ij} is a useful way to reveal the relevant correlation lengths without requiring explicit measurement of multispin correlations.

[1] M. D. Ediger, C. A. Angell, and S. R. Nagel, J. Phys. Chem. **100**, 13200 (1996).
[2] P. G. Debenedetti and F. H. Stillinger, Nature (London) **410**, 259 (2001).
[3] L. Berthier and G. Biroli, Rev. Mod. Phys. **83**, 587 (2011).
[4] J.-P. Bouchaud and G. Biroli, J. Chem. Phys. **121**, 7347 (2004).
[5] A. Montanari and G. Semerjian, J. Stat. Phys. **125**, 22 (2006).
[6] J. Kurchan and D. Levine, J. Phys. A **44**, 035001 (2011).
[7] A. Cavagna, T. S. Grigera, and P. Verrocchio, Phys. Rev. Lett. **98**, 187801 (2007).
[8] G. Biroli, J.-P. Bouchaud, A. Cavagna, T. S. Grigera, and P. Verrocchio, Nat. Phys. **4**, 771 (2008).
[9] W. Kob, S. Roldan-Vargas, and L. Berthier, Nature Phys. **8**, 164 (2012).
[10] *Dynamical Heterogeneities in Glasses, Colloids, and Granular Media*, edited by L. Berthier, G. Biroli, J.-P. Bouchaud, L. Cipelletti, and W. van Saarloos (Oxford University Press, Oxford, 2011).
[11] L. Berthier and W. Kob, Phys. Rev. E **85**, 011102 (2012).
[12] C. Cammarota and G. Biroli, eprint arXiv:1106.5513 (to be published).
[13] A. Lipowski, J. Phys. A **30**, 7365 (1997).
[14] M. E. J. Newman and C. Moore, Phys. Rev. E **60**, 5068 (1999).
[15] J. P. Garrahan, J. Phys. Condens. Matter **14**, 1571 (2002).
[16] R. L. Jack, L. Berthier, and J. P. Garrahan, Phys. Rev. E **72**, 016103 (2005).
[17] R. L. Jack and J. P. Garrahan, J. Chem. Phys. **123**, 164508 (2005).
[18] A. Buhot and J. P. Garrahan, Phys. Rev. Lett. **88**, 225702 (2002).
[19] R. L. Jack, L. Berthier, and J. P. Garrahan, J. Stat. Mech. (2006) P12005.
[20] F. Sausset and D. Levine, Phys. Rev. Lett. **107**, 045501 (2011).
[21] P. Ronhovde, S. Chakrabarty, D. Hu, M. Sahu, K. Sahu, K. Kelton, N. Mauro, and Z. Nussinov, Eur. Phys. J. E **34**, 105 (2011).
[22] P. Ronhovde, S. Chakrabarty, D. Hu, M. Sahu, K. Sahu, K. Kelton, N. Mauro, and Z. Nussinov, eprint arXiv:1101.0008 (to be published).
[23] K. Kim, Europhys. Lett. **61**, 790 (2003).
[24] S. Karmakar, E. Lerner, and I. Procaccia, Physica A **391** 1001 (2012).
[25] B. Charbonneau, P. Charbonneau, and G. Tarjus, Phys. Rev. Lett. **108**, 035701 (2012).
[26] T. R. Kirkpatrick and D. Thirumalai, Phys. Rev. B **36**, 5388 (1987).
[27] T. R. Kirkpatrick, D. Thirumalai, and P. G. Wolynes, Phys. Rev. A **40**, 1045 (1989).
[28] V. Krakoviack, Phys. Rev. E **84**, 050501 (2011).
[29] D. Kivelson, S. A. Kivelson, X. L. Zhao, Z. Nussinov, and G. Tarjus, Physica A **219**, 27 (1995).
[30] G. Tarjus, S. A. Kivelson, Z. Nussinov, and P. Viot, J. Phys. Condens. Matter **17**, R1143 (2005).
[31] F. Ritort and P. Sollich, Adv. Phys. **52**, 219 (2003).
[32] D. Chandler and J. P. Garrahan, Annu. Rev. Phys. Chem. **61**, 191 (2010).
[33] J. P. Garrahan and D. Chandler, Proc. Natl. Acad. Sci. USA **100**, 9710 (2003).
[34] L. Berthier and J. P. Garrahan, J. Phys. Chem. B **109**, 3578 (2005).
[35] A. S. Keys, L. O. Hedges, J. P. Garrahan, S. C. Glotzer, and D. Chandler, Phys. Rev. X **1**, 021013 (2011).
[36] S. Sasa, J. Phys. A **43**, 465002 (2010).
[37] K. Kim, K. Miyazaki, and S. Saito, J. Phys. Condens. Matter **23**, 234123 (2011).
[38] L. Berthier, G. Biroli, J.-P. Bouchaud, W. Kob, K. Miyazaki, and D. R. Reichman, J. Chem. Phys. **126**, 184503 (2007).
[39] L. Berthier, G. Biroli, J.-P. Bouchaud, W. Kob, K. Miyazaki, and D. R. Reichman, J. Chem. Phys. **126**, 184504 (2007).
[40] L. Berthier, G. Biroli, J. Bouchaud, L. Cipelletti, D. El Masri, D. L'Hote, F. Ladieu, and M. Pierno, Science **310**, 1797 (2005).
[41] V. Krakoviack, Phys. Rev. E **82**, 061501 (2010).
[42] A. Widmer-Cooper, P. Harrowell, and H. Fynewever, Phys. Rev. Lett. **93**, 135701 (2004).
[43] A. Widmer-Cooper and P. Harrowell, J. Chem. Phys. **126**, 154503 (2007).
[44] C. Cammarota, G. Biroli, M. Tarzia, and G. Tarjus, Phys. Rev. Lett. **106**, 115705 (2011).
[45] M. Castellana, Europhys. Lett. **95**, 47014 (2011).
[46] J. Yeo and M. A. Moore, eprint arXiv:1111.3105 (to be published).
[47] M. C. Angelini, G. Parisi and F. Ricci-Tersenghi, eprint arXiv:1111.6869 (to be published).
[48] L. Berthier and R. L. Jack, Phys. Rev. E **76**, 041509 (2007).